Thermionic Emission Dynamics of Ultrafast Electron Sources

Chao-Yu Guo(郭钞宇)[1†], Hao-Tian Zheng(郑浩天)[1†], Gui-Lin Zhu(朱贵林)[5†], Yu-Qing Huang(黄玉清)[1], Qin Wang(王钦)[1], Da Wu(吴达)[1], Zheng-Pu Zhao(赵正朴)[1], Chu-Wei Zhang(张楚惟)[1], Jing-Tao Lü(吕京涛)[5*] and Ying Jiang(江颖)[1,2,3,4*]

[1]*International Center for Quantum Materials, School of Physics, Peking University, Beijing 100871, China*
[2]*Collaborative Innovation Center of Quantum Matter, Beijing 100871, China*
[3]*Interdisciplinary Institute of Light-Element Quantum Materials and Research Center for Light-Element Advanced Materials, Peking University, Beijing 100871, China*
[4]*New Cornerstone Science Laboratory, Peking University, Beijing 100871, China*
[5]*School of Physics, Huazhong University of Science and Technology, Wuhan 430074, China*

(Received 25 February 2025; accepted manuscript online 14 April 2025)

Ultrafast electron sources, which enable high spatiotemporal resolution in time-resolved electron microscopy and scanning probe microscopy, are receiving increased attention. The most widely used method for achieving ultrafast electron sources involves irradiating metal tips by ultrashort laser pulses, causing electron beam emission via the photoelectric effect [including photon-driven (quantum) or field-driven (classical) emission]. However, the thermionic electrons emission process due to the heating effect of ultrashort lasers, particularly its dynamic aspects, has rarely been addressed in previous studies. In this paper, we improved the signal-to-noise ratio of a two-pulse correlation measurement on the tip electron emission by nearly two orders of magnitude using a delay time modulation method. This allowed us to obtain information on the temperature evolution of hot electrons and phonons in a non-equilibrium state, and to extract characteristic time scales for electron-phonon and phonon-phonon scattering. Our findings indicate that the thermionic electrons emission, unlike the instantaneous photoelectric effect, causes electron emission to lag behind the laser pulse by tens of picoseconds, thus significantly affecting the detection of ultrafast dynamics of samples. Furthermore, such a lagging effect was found to be sensitive to the local structure of the metal tip, offering new insights into the improved design of ultrafast electron sources.

DOI: 10.1088/0256-307X/42/5/057503 CSTR: 32039.14.0256-307X.42.5.057503

To investigate ultrafast dynamics with high spatiotemporal resolution, substantial progress have been made in developing methods such as ultrafast scanning electron microscopy (SEM),[1–3] ultrafast transmission electron microscopy (TEM),[4–9] and time-resolved scanning tunneling microscopy (STM).[10–15] Ultrafast electron sources are the cornerstone of these new methods. The spatial localization and temporal duration of the electron pulses are critical for the spatiotemporal resolution. Typically, ultrafast electron beams are produced by irradiating sharp metal tips with ultrashort laser pulses. However, the interaction of the laser pulses with the sharp tip and the electron emission mechanism are not yet fully understood.

When a focused pulsed laser illuminates the tip, there are two main mechanisms for metal surface photoemission. The first is photon-driven or field-driven emission. For relatively weak fields, single electrons excited by single or multiphoton absorption escape when their energy exceeds the work function of the sample. Under strong field conditions, the optical field is sufficiently strong to deform the vacuum barrier, liberating free electrons from the metal surface. The second mechanism involves laser-induced thermal effects. Upon excitation, hot electrons with energy above the Fermi level are generated. Through electron-electron collisions, Auger recombination and electron-phonon scattering, these hot electrons quickly[16–20] (within 10–100 fs) enter a thermalized regime, where their energy distribution can be described by a high-temperature Fermi–Dirac distribution. The emission behavior of electrons in this regime is termed thermionic emission [Fig. 1(b)].[21] Thus, whether the energy distribution of emitted electrons fits the Fermi–Dirac distribution can be used as an indicator for the thermionic emission process. However, the photocurrent signal of thermionic emission dynamics is usually very weak. The thermionic emission dynamics has rarely been addressed in previous studies due to the limitation of signal-to-noise ratio by conventional pump-probe techniques. Electron pulses undergo space-charge (Coulomb repulsion) broadening effect[22] during propagation, for example, the electron pulse of 100 fs-duration experienced degradation to the picosecond domain during pulse propagation for hundreds of micrometers. Electron pulse broadening can significantly distort the electron energy distribution. Utilizing STM,

†These authors contributed equally to this work.
*Corresponding author. Email: yjiang@pku.edu.cn; jtlu@hust.edu.cn
© 2025 Chinese Physical Society and IOP Publishing Ltd. All rights, including for text and data mining, AI training, and similar technologies, are reserved.

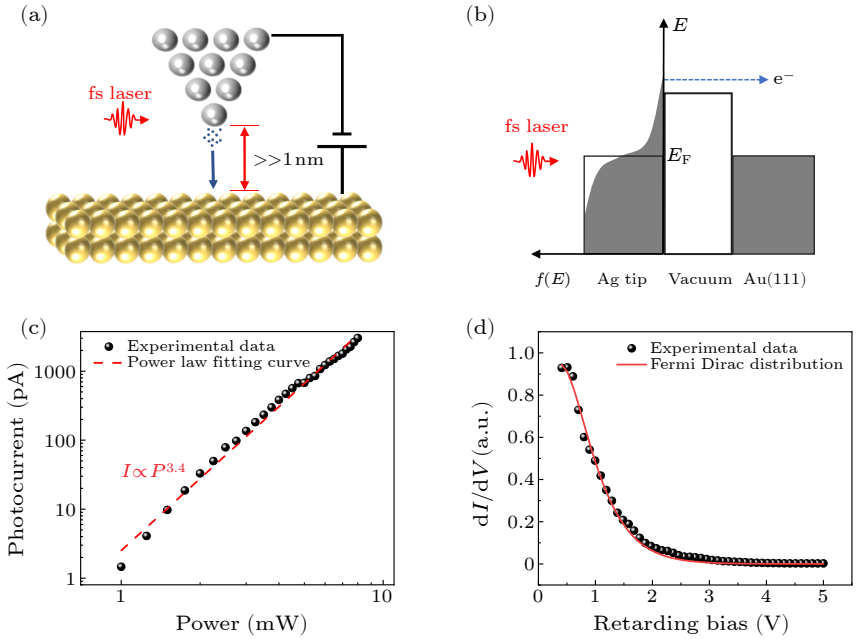

Fig. 1. Steady state of STM tip photoemission. (a) Schematic diagram of the experimental setup. (b) Schematic of the thermionic emission. (c) Dependence of the photocurrent on laser power at 700-nm wavelength. (d) The dI/dV spectrum of photocurrent at 2 mW, reflecting the energy distribution of photoelectrons.

the distance between the tip and the anode can be reduced to less than 50 nm, effectively eliminating the influence of space-charge broadening. Moreover, a smaller tip-anode separation facilitates the collection of electrons from a wider range of emission angles.

Figure 1(a) depicts a schematic diagram of the experiment performed with a homemade ultrahigh vacuum (base pressure better than 2×10^{-10} mbar) cryogenic (5 K) STM system. Photoelectron emission from electrochemically etched polycrystalline silver tips was triggered by 100 fs laser pulses, with a central wavelength of 700 nm and a repetition rate of 80 MHz from a Ti:sapphire ultrafast laser (SpectraPhysics, Mai Tai-Series, SHG). The anode is a Au(111) single crystal (MaTech). With the help of an aspheric lens (Edmund Optics, EFL = 20 mm, N.A. = 0.38), the laser spot can be precisely focused on the tip with a diameter smaller than 10 μm. The bias voltage refers to the sample (anode) voltage with respect to the tip. The tip-surface distance was set beyond the tunneling region (∼1 nm), which can eliminate the tunneling current and meanwhile maximize the photoelectron emission current.

In our experiments, photoemission currents (I) were recorded as a function of incident laser power (P) under a bias voltage of 5 V, as shown in Fig. 1(c). The emission current was approximately proportional to the cube of laser power ($I \propto P^{3.4}$), suggesting multiphoton photoemission. The work function (φ) of the silver tip (≈4.26 eV) requires at least three photons for photoemission, which is consistent with the experimental data. Therefore, the three-photon absorption process in our experiment is the dominant one.

The energy distribution of emitted electron beams can be measured using the retarding field method, where the bias voltage (V_b) is scanned while the photocurrent intensity is recorded.[23] When the retarding field (negative bias) is large enough, electrons lack the kinetic energy to overcome the retarding potential and thus cannot reach the anode, resulting in a diminishing photocurrent. As the retarding field weakens, electrons with kinetic energy greater than the retarding potential can reach the anode, contributing to the photocurrent. Therefore, the energy distribution of photoelectrons can be directly obtained from the differential spectrum of $I(V_b)$. For Fig. 1(d), using Fermi–Dirac fitting,[24] an initial electron temperature of 4000 K provides a good fit.[25,26] This indicates that the thermionic emission process plays an important role in the photocurrent generation.

Unlike the instantaneous nature of multiphoton photoemission (MPP), where the electron beam is mainly concentrated within the laser pulse duration,[27,28] thermionic emission, due to the gradual cooling of electron temperature, results in electron emission lagging behind the laser pulse [Fig. 3(c)], broadens the emitted electron pulse and thus affecting the temporal resolution of dynamic detection.[29,30] To investigate the dynamics of photoelectron emission, we employed a two-pulse correlation measurement method.[31,32] The first light pulse induces photoelectron emission and rapidly increases the electron temperature. If the hot electrons have not completely cooled, a second laser pulse of the same power will produce a larger photocurrent. By varying the delay time between the two pulses and recording the total photocurrent, we can extract the relaxation dynamics of electron temperature.

To enhance the signal-to-noise ratio, we typically modulate the laser power using a chopper and read out the signal with a lock-in amplifier. As shown in Fig. 2(a), when the delay time between the two pulses is less than the laser pulse width, the two pulses interfere,

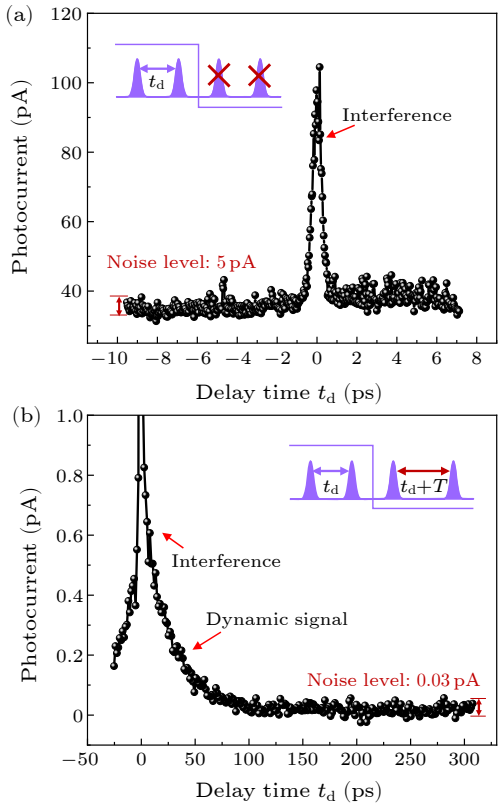

Fig. 2. Two-pulse correlation curves measured by different modulation methods. (a) Measurement by chopper modulation. Laser power: 18 mW, lock-in sensitivity: 200 mV. (b) Measurement by delay time modulation. Laser power: 8 mW, lock-in sensitivity: 20 mV. Temperature: 77 K, wavelength: 450 nm, integration time: 200 ms, bias: 5 V.

creating a photocurrent autocorrelation curve. This indicates the instantaneous nature of the multiphoton emission process. When the delay time exceeds the laser pulse width, the total photocurrent signal is buried in the background noise, primarily resulting from capacitance changes[33] caused by the thermal expansion and contraction of the tip (noise level: ∼5 pA), prohibiting the dynamic measurements of thermionic emission. To extract the weak dynamic signals of thermionic emission, we developed an advanced delay-time modulation technique.[34] By alternately selecting odd or even numbers of laser pulses, an AC modulation (T) was introduced to the delay time (t_d) at a specific modulation frequency [inset in Fig. 2(b)]. This method maintained a constant average laser power, which allowed the suppression of tip thermal noise. As a result, the photocurrent noise level was significantly improved by almost two orders of magnitude (∼0.03 pA). With the help of a lock-in amplifier, the weak dynamic signal can be extracted from the background noise. When T is set to a value sufficiently large (around 12.5 ns), the electron temperature can fully cool down to its initial state. The output of lock-in amplifier can be simply interpreted as the difference between the photocurrent at the highest electron temperature and the initial temperature. This two-pulse correlation measurement is sensitive to the population of hot electron and clearly reveals the picosecond-scale emission signals.

Upon detailed examination, the photocurrent as a function of the delay time exhibits biexponential characteristics, as shown in Fig. 3(a). Through fitting, we identified a faster decay constant of approximately 2 ps, consistent with the typical electron-phonon scattering time scale for most materials (1–10 ps).[35–37] The slower decay constant of 26 ps corresponds to the cooling process via scattering between different phonon modes.[17,38] The dynamic process of hot electron cooling, following the ultrashort laser excitation, is illustrated in Fig. 3(b). Initially, the hot electrons quickly enter a thermalized regime within 10–100 fs, forming a Fermi–Dirac distribution. Electrons with energy above the work function can escape the surface, generating a photocurrent. Subsequently, hot electrons dissipate energy through electron-phonon coupling. As the phonon

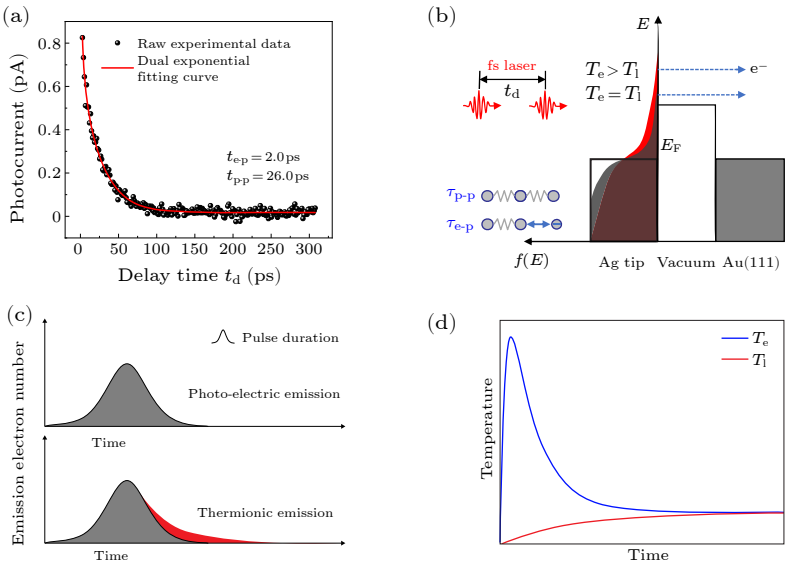

Fig. 3. Tip photoemission dynamics. (a) Fitting of the tip photoemission relaxation dynamics. (b) The relaxation process of optically excited hot electrons in Ag tip through electron-phonon and phonon-phonon interactions. (c) Difference between photoelectric emission and thermionic emission. (d) Schematic of electron and phonon temperature evolution.

temperature (lattice temperature T_l) rises, the electron temperature T_e gradually decreases until the thermal equilibrium between T_l and T_e is achieved. Concurrently, the number of electrons contributing to the photocurrent diminishes as T_e decreases, from which the characteristic time of electron-phonon scattering can be extracted [Fig. 3(d)]. After the thermal equilibrium between electron and phonon temperatures is established, the phonon-phonon scattering contributes to further reduction of electron temperature. Therefore, the temporal evolution signal of the photocurrent accurately reflects the dynamics of electron-phonon and phonon-phonon scattering processes.

Since the intensity of thermionic current is much lower than that of multiphoton emission, the electron pulse width is essentially consistent with the laser pulse width, as shown in Fig. 2(a). However, as an ultrafast electron source, the picosecond-scale thermionic lagging emission can still affect the detection of dynamic signals, particularly for weak signals. We found experimentally a strong dependence of the thermionic emission dynamics on the local structure of the tip. Near the tip apex, where the radius of curvature is small, both the electron-phonon and phonon-phonon scattering processes are faster [Fig. 4(a)] than these processes away from the tip apex [Fig. 4(b)]. Upon exposure to ultrashort laser pulses, the tip apex experiences a strong local field enhancement due to the lightning-rod effect or surface plasmon effect,[39] resulting in higher electron temperature. Such an electron temperature difference induced by the local field effect may affect the electron-phonon and phonon-phonon scattering rates.

To confirm this assumption, we calculated the electron-phonon and phonon-phonon interactions using Density Functional Theory.[40,41] The calculated average scattering rates for electron-phonon and phonon-phonon interactions as a function of temperature is shown in Figs. 4(c) and 4(d), respectively. Notably, the electron-phonon scattering rate exhibits a strong temperature dependence, showing that the scattering rate increases as the temperature rises. The inset in Fig. 4(d) displays the dispersion of three phonon branches. The scattering rates for the three phonon branches show a similar trend in their response to temperature changes. At higher temperatures, the phonon-phonon scattering rate increases dramatically, which is consistent with the experimental results. However, the deduced characteristic time for the electron-phonon and phonon-phonon scattering (τ_ep and τ_pp) are much smaller than the experimental results. This discrepancy may be attributed to the unknown geometry of the realistic silver tip in experiment, which can significantly impact the scattering rates. Our findings suggest that the lagging emission of thermionic electrons can be suppressed by optimizing the local structure at the tip apex, such as constructing plasmonic junctions with high electron temperatures.

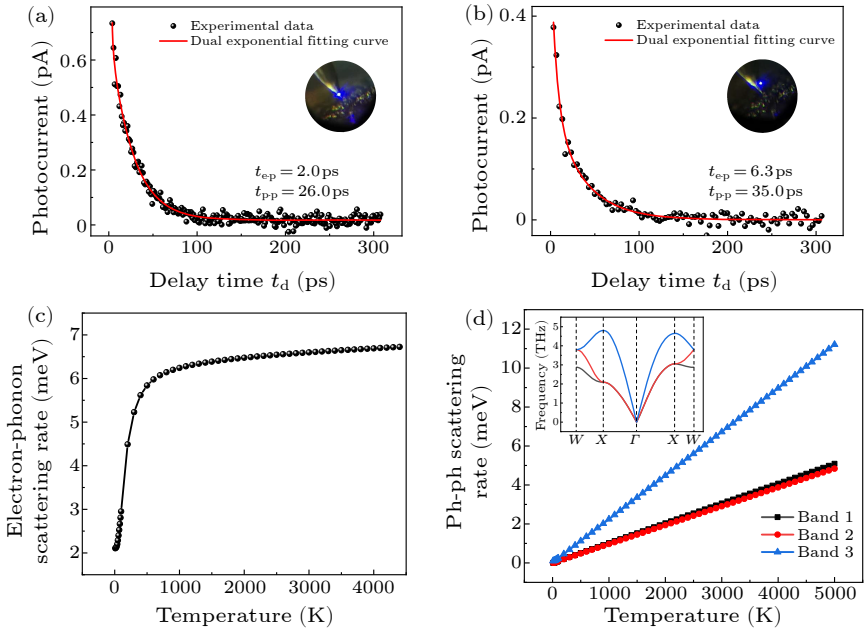

Fig. 4. Correlation between laser focusing sites and relaxation dynamics. (a) and (b) The relaxation dynamics when the laser focus is at the tip apex and away from the tip apex, respectively. The inset shows the laser irradiation sites on the tip. (c) and (d) The calculated average scattering rates for electron-phonon and phonon-phonon interactions as a function of temperature, respectively. The inset shows the dispersion spectrum of three phonon branches.

In summary, this work provides ultrafast dynamics for electrons and phonons in the thermionic emission process and extracts characteristic time scales for electron-phonon and phonon-phonon scattering. This tens-of-picoseconds lagging electron emission significantly affects the temporal resolution of dynamics detection, especially when the dynamics signal is weak. Furthermore, the electron pulse lagging was found to be sensitive to the local structure of the metal tip, offering new guidelines for optimizing the design of ultrafast electron sources. Additionally, our approach to studying electron-phonon scattering can be extended to other systems that exhibit electron-phonon

coupling.

Acknowledgements. This work was supported by the National Key R&D Program under Grant No. 2021YFA1400500, the National Natural Science Foundation of China under Grant No. 22273029. Y.J. acknowledges the New Cornerstone Science Foundation through the New Cornerstone Investigator Program under Grant No. NCI202303 and the XPLORER PRIZE, and the Beijing Outstanding Young Scientist Program under Grant No. JWZQ20240101002.

References

[1] Mohammed O F, Yang D S, Pal S K, and Zewail A H 2011 *J. Am. Chem. Soc.* **133** 7708
[2] Kozák M, McNeur J, Schönenberger N, Illmer J, Li A, Tafel A, Yousefi P, Eckstein T, and Hommelhoff P 2018 *J. Appl. Phys.* **124** 023104
[3] Yang D S, Mohammed O F, and Zewail A H 2010 *Proc. Natl. Acad. Sci. U.S.A.* **107** 14993
[4] Danz T, Domröse T, and Ropers C 2021 *Science* **371** 371
[5] Hassan M T, Baskin J S, Liao B, and Zewail A H 2017 *Nat. Photonics* **11** 425
[6] Priebe K E, Rathje C, Yalunin S V, Hohage T, Feist A, Schäfer S, and Ropers C 2017 *Nat. Photonics* **11** 793
[7] Zewail A H 2010 *Science* **328** 187
[8] Zhang Y C and Flannigan D J 2019 *Nano Lett.* **19** 8216
[9] Houdellier F, Caruso G M, Weber S, Kociak M, and Arbouet A 2018 *Ultramicroscopy* **186** 128
[10] Terada Y, Yoshida S, Takeuchi O, and Shigekawa H 2010 *Nat. Photonics* **4** 869
[11] Garg M and Kern K 2020 *Science* **367** 411
[12] Kloth P and Wenderoth M 2017 *Sci. Adv.* **3** e1601552
[13] Cocker T L, Jelic V, Gupta M, Molesky S J, Burgess J A J, De Los Reyes G, Titova L V, Tsui Y Y, Freeman M R, and Hegmann F A 2013 *Nat. Photonics* **7** 620
[14] Cocker T L, Peller D, Yu P, Repp J, and Huber R 2016 *Nature* **539** 263
[15] Guo C Y, Meng X Z, Fu H X, Wang Q, Wang H M, Tian Y, Peng J B, Ma R Z, Weng Y X, Meng S, Wang E G, and Jiang Y 2020 *Phys. Rev. Lett.* **124** 206801
[16] Khakshouri S, Alfè D, and Duffy D M 2008 *Phys. Rev. B* **78** 224304
[17] Caruso F and Novko D 2022 *Adv. Phys. X* **7** 2095925
[18] Mueller B Y and Rethfeld B 2013 *Phys. Rev. B* **87** 035139
[19] Bennemann K H 2004 *J. Phys.: Condens. Matter* **16** R995
[20] Lisowski M, Loukakos P A, Bovensiepen U, Stähler J, Gahl C, and Wolf M 2004 *Appl. Phys. A* **78** 165
[21] Herring C and Nichols M H 1949 *Rev. Mod. Phys.* **21** 185
[22] Cao J, Hao Z, Park H, Tao C, Kau D, and Blaszczyk L 2003 *Appl. Phys. Lett.* **83** 1044
[23] Li C, Zhou X, Zhai F, Li Z J, Yao F R, Qiao R X, Chen K, Cole M T, Yu D P, Sun Z P, Liu K H, and Dai Q 2017 *Adv. Mater.* **29** 1701580
[24] DuBridge L A 1933 *Phys. Rev.* **43** 727
[25] Riffe D M, Wang X Y, Downer M C, Fisher D L, Tajima T, Erskine J L, and More R M 1993 *J. Opt. Soc. Am. B* **10** 1424
[26] Johannsen J C, Ulstrup S, Cilento F, Crepaldi A, Zacchigna M, Cacho C, Turcu I C E, Springate E, Fromm F, Raidel C, Seyller T, Parmigiani F, Grioni M, and Hofmann P 2013 *Phys. Rev. Lett.* **111** 027403
[27] Aidelsburger M, Kirchner F O, Krausz F, and Baum P 2010 *P Natl. Acad. Sci. USA* **107** 19714
[28] Barwick B, Corder C, Strohaber J, Chandler-Smith N, Uiterwaal C, and Batelaan H 2007 *New J Phys.* **9** 142
[29] Sabanés N M, Krecinic F, Kumagai T, Schulz F, Wolf M, and Müller M 2022 *ACS Nano* **16** 14479
[30] Kealhofer C, Foreman S M, Gerlich S, and Kasevich M A 2012 *Phys. Rev. B* **86** 035405
[31] Huang Y Q, Guo C Y, Gao L, Du W N, Zheng H T, Wu D, Zhao Z P, Zhang C W, Wang Q, Liu X F, Yan Q F, and Jiang Y 2024 *Chin. Phys. B* **33** 107304
[32] Wang H N, Zhang C J, Chan W M, Tiwari S, and Rana F 2015 *Nat. Commun.* **6** 8831
[33] Kurokawa S and Sakai A 1998 *J. Appl. Phys.* **83** 7416
[34] Takeuchi O, Morita R, Yamashita M, and Shigekawa H 2002 *Jpn. J. Appl. Phys.* **41** 4994
[35] Kampfrath T, Perfetti L, Schapper F, Frischkorn C, and Wolf M 2005 *Phys. Rev. Lett.* **95** 187403
[36] Pogna E A A, Jia X Y, Principi A, Block A, Banszerus L, Zhang J C, Liu X T, Sohier T, Forti S, Soundarapandian K, Terrés B, Mehew J D, Trovatello C, Coletti C, Koppens F H L, Bonn M, Wang H I, van Hulst N, Verstraete M J, Peng H L, Liu Z F, Stampfer C, Cerullo G, and Tielrooij K J 2021 *ACS Nano* **15** 11285
[37] Wu S W, Liu W T, Liang X G, Schuck P J, Wang F, Shen Y R, and Salmeron M 2012 *Nano Lett.* **12** 5495
[38] Mo M Z, Tamm A, Metsanurk E, Chen Z J, Wang L, Frost M, Hartley N J, Ji F H, Pandolfi S, Reid A H, Sun P H, Shen X Z, Wang Y Q, Wang X J, Glenzer S, and Correa A A 2024 *Sci. Adv.* **10** eadk9051
[39] Urbieta M, Barbry M, Zhang Y, Koval P, Sánchez-Portal D, Zabala N, and Aizpurua J 2018 *ACS Nano* **12** 585
[40] Wang Y, Lu Z X, and Ruan X L 2016 *J. Appl. Phys.* **119** 225109
[41] Xu M, Yang J Y, Zhang S Y, and Liu L H 2017 *Phys. Rev. B* **96** 115154